文章编号:1000-0887(2016)12-1394-09
ⓒ 应用数学和力学编委会,ISSN 1000-0887

Study on the Nozzle Jet in Arc Spraying*

TAMAKI Ryoji[1], YAMAKAWA Masashi[2]
(1. *Daihen Co., Ltd.*, *Koyocho-nishi*, *Higashinada-ku*, *Kobe Hyogo* 6580033, *Japan*;
2. *Kyoto Institute of Technology*, *Matsugasaki*, *Sakyo-ku*, *Kyoto* 6068585, *Japan*)

Abstract: The jet plume formed immediately adjacent to the nozzle of an arc spray gun has a significant effect on the properties of the resultant coating. This study applied the computational fluid dynamics (CFD) and the Schlieren photography to elucidate the properties of jet plumes. The Schlieren images examined revealed that the properties and widths of the plume depend on the direction of material wires for thermal coating. Through the CFD approach, we observed the formation of shock waves immediately after the nozzle aperture and damping of the shock waves in the downstream plume.

Key words: arc spraying; shock wave; compression; expansion
CLC number: O35 **Document code**: A
doi: 10.21656/1000-0887.370554

Introduction

In metal hardware industries, the coating processes called thermal spraying are widely used to repair surfaces of mechanical components, increase hardness, and provide rust and corrosion protection to outdoor structural materials such as iron beams for bridges. Thermal spray coating technologies are coating processes in which melted materials are sprayed onto a surface.

Various methods exist for thermal spray coating, though, they are roughly classified into 2 as shown in fig. 1 according to the method employed to heat coating materials to molten or semi-molten state. The oxy-fuel spraying is subdivided into flame spraying and high-velocity flame spraying. The former utilizes a gas mixture of oxygen and acetylene as a heat source to produce combustion flame together with compressed air to accelerate material globules in the form of micrometer-size particles toward work pieces. The high-velocity oxy-fuel (HVOF) coating, an other subset of flame spraying, utilizes high-pressure oxygen to produce confined combustion at high pressures and hot gas flame jet that accelerates globules toward work pieces at extreme velocities.

The electric spraying includes the plasma spraying and the electric arc spraying, which is the subject of this study. For the plasma spraying, the plasma gas at a high temperature and a high velocity is used as the heat source. In a plasma-arc gun, an inert gas, typically

* Received 2016-11-05; Revised 2016-11-25
Corresponding author, TAMAKI Ryoji, E-mail: tamaki@daihen.co.jp

argon, is charged by electrodes and ionized to generate hot, high-velocity plasma. Usually, with a water-cooled copper the plasma is created by an electric arc burning within the nozzle of a plasma gun and the arc gas is formed into a plasma jet as it emerges from the nozzle. Powder particles are injected into this jet and then strike the surface of the work piece at high velocity to produce a strongly adherent coating.

The wire arc spraying is a form of thermal spraying where 2 metal wires which ultimately form the coating are fed independently into the spray gun as shown in fig. 2. Typical wire arc spray materials are aluminum/zinc, copper/copper, and steel/steel for example. These wires are fed into a device called wire feeding unit and electrically charged via electrodes to generate an arc. The wires are faced together and form an electric arc that melts the wires. Compressed air or other gas, passing through a nozzle, atomizes the molten metal and sprays it onto the substrate surface. Among the methods described above, the wire arc spraying produces the fastest coating rates with relatively high quality, therefore, is capable of coating in bulk within a short time. The advantage of cost effectiveness contributes to the wide use of the wire arc spraying across industries. The advantage of the wire arc spraying includes that both the initial cost and the running cost are lower than those needed for the plasma spray method.

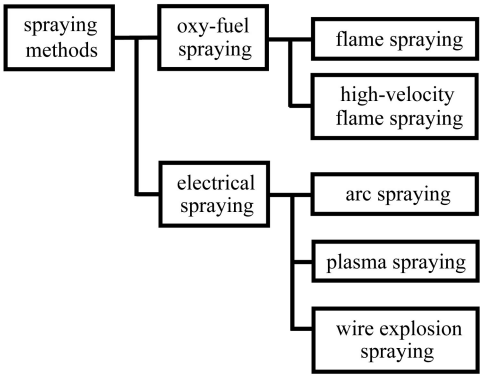

Fig. 1 The spraying methods

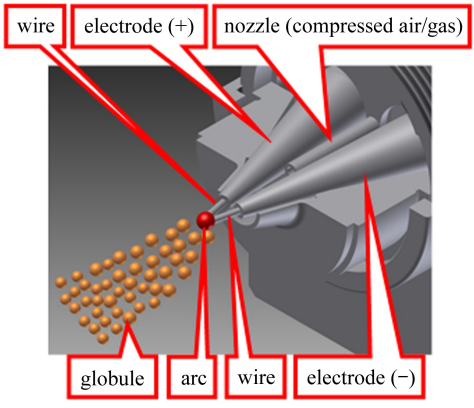

Fig. 2 The wire arc spraying system

The wire spraying method, however, has some disadvantages. Advantages and disadvantages of this method are listed in table 1. Because material globules in a molten state are entrained in an air jet and oxidized before being deposited onto a substrate, the resulting coating is subject to entrained oxides to some extent. Globules in a jet air may generate a substantial amount of fine dust (fume) that results in contaminants in the coating produced. Another disadvantage of the wire arc sprayed coatings is that they are susceptible to the formation of voids and detachments that are found across the entire coating thickness. The percentage of these voids and detachments in a cross-sectioned coating is referred to as area percent porosity, and depending on application, higher porosity is considered intolerable. That is, when wear resistance is the purpose of a thermal sprayed coat-

ing, voids contained in the coating effectively hold lubricant, however, high porosity is considered unsuitable for a coating intended to prevent rust and corrosion since corrosive liquids and gases can penetrate the coating and come in contact with the substrate/coating interface. Thermal spray coating suppliers have been seeking for optimal setup of coating control process parameters for each application together with the use of fume collectors to control porosity. However, there has been no drastic solution, and issues remain for effective porosity control.

Many studies have been conducted to establish a reliable method for characterization of properties of electric/wire arc spraying phenomena. Consider, for example, studies conducted by Watanabe and Kawase et al.[1-5] used air, oxygen, nitrogen, and argon to atomize and spray the melted particles to reveal the effect of compressed gas on the particle oxidation. According to their study, in nitrogen and argon, oxidation accelerates as molten particles' diameters decrease due to increased arc temperature[1]. Kawase et al. characterized the changes in the adhesion of coatings processed under varied feeding rates and arc voltages with aluminum and stainless steel wires. They further dug deeper in the arc spraying phenomena and properties of melted particles in air jet with a high-speed camera[2-5].

The above studies conducted to date have elucidated the effects of variable arc spraying parameters (e.g., arc voltage, wire feeding rate, type of compressed gas) on the properties of resultant coatings. However, it is hard to say that the effect of a compressed gas jet, i.e., the plume of fluid, on arc spraying has been well elucidated. In the present paper, we aim to clarify the properties of the jet plume that takes place in the wire arc spraying process and use the flow visualization technique known as the Schlieren photography to capture jet plumes. Numerical simulation is used as well to cover the flow of fluid thresholded by the Schlieren photography.

Table 1 Advantages and disadvantages of the wire arc spraying

advantage	disadvantage
• low initial cost for equipment installation • low running cost and capability of spraying in bulk within short time • produces relatively high quality coating	• susceptible to oxide entrainment • generates a lot of fume (atomized particles) that can be entrained into coating

Note Generates a lot of voids and detachments in coating (whether or not high porosity is beneficial depends on the application of coating).

1 Schlieren photography

1.1 Method

Before the computational fluid dynamics analysis, the jet plume is visualized with the Schlieren photography to see the phenomena. Fig. 3 illustrates the principles of the Schlieren method. Slight variations in refractive indices caused by density gradients in the fluid distort the collimated light beam. The Schlieren method visualizes fluid distort, relying on

the fact that light rays are bent whenever they encounter changes in density of a fluid. In this experiment, the density distribution of compressed air is observed in the form of light contrast. The system has a component called a knife edge that cuts off the fluid distort to provide clear visualization of the jet plume.

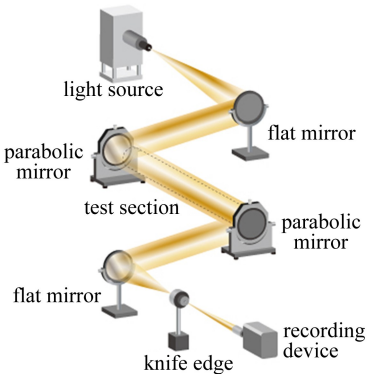

Fig. 3 The Schlieren principle diagram[6]

1.2 Experimental system

The configuration of the system used for the experiment is given in fig. 4. The system is equipped with a prototype thermal spray gun having a 6 mm diameter nozzle that designed based on ASTS-2501 torch manufactured by Daihen. A compressor was used for the air jet. The air was allowed to flow in the line with a flowmeter, a regulator with pressure gauge and an air tank, and the gun placed in this order from upstream. Air pressures and temperatures at the tank were measured simultaneously. Ambient temperatures in the lab were also monitored.

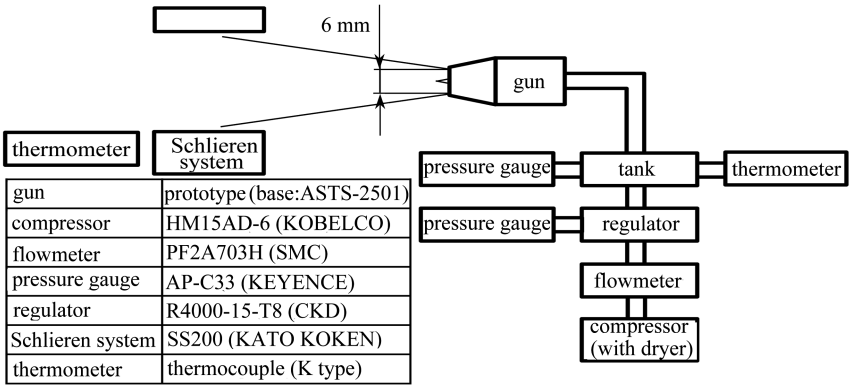

gun	prototype (base:ASTS-2501)
compressor	HM15AD-6 (KOBELCO)
flowmeter	PF2A703H (SMC)
pressure gauge	AP-C33 (KEYENCE)
regulator	R4000-15-T8 (CKD)
Schlieren system	SS200 (KATO KOKEN)
thermometer	thermocouple (K type)

Fig. 4 The experimental system

1.3 Results of Schlieren photography

Fig. 5 provides the results of Schlieren photography carried out under tank pressures ranging from 0.2 to 0.5 MPa. The tank pressure values are those measured at the pressure gauge. The wires were positioned so they were fed in the direction shown in fig. 6. On the Schlieren image taken at 0.2 MPa tank pressure, the formation of faint shock waves is seen. As the tank pressure increases, longer shock waves are formed downstream; howev-

er, the formation is still unclear.

The plumes may have been affected by the wire position when the images were taken. So, we made a 90° rotation for the shooting position shown in fig. 6 and performed another round of plume visualization. That is, the wires were fed in the direction shown in fig. 7. Fig. 8 provides the results of Schlieren photography after the shooting position rotation. As is seen on the Schlieren image taken at 0.2 MPa tank pressure, the formation of shock waves is observed at the wire tips. As the tank pressure increases, shock waves in the upper and lower regions of the wires become clearer. The image of the plume at 0.5 MPa indicates that the shock wave formation reaches the 6th cell in the pane. The plumes in fig. 8 are wider than those shown in fig. 5. It is considered that the difference is attributed to the formation of shock waves that take place in the upper and lower regions of the wires.

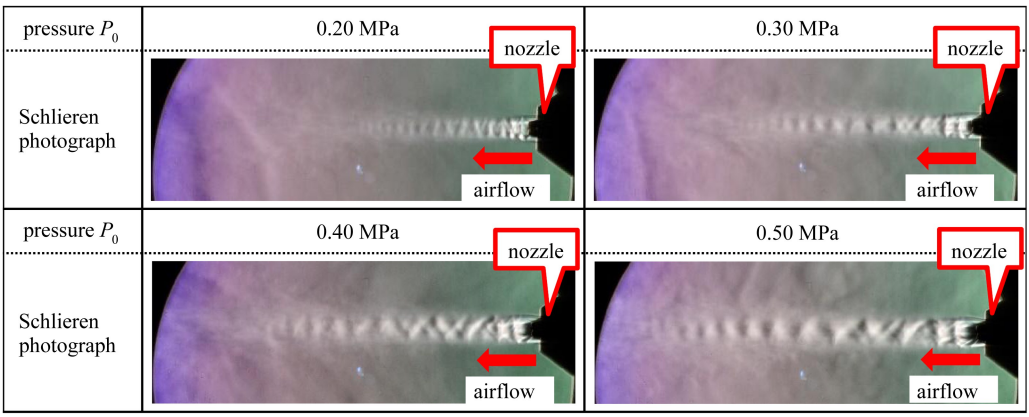

Fig. 5 Schlieren photograph

The Schlieren photography provided some of the properties of the plumes phenomena. To dig deeper in details of wire arc spraying plumes, we carried out CFD analysis.

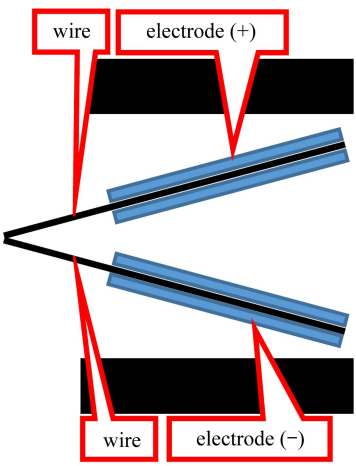

Fig. 6 The wire direction

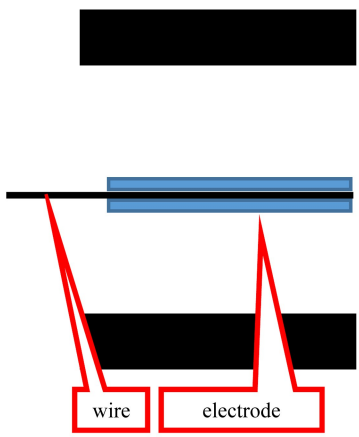

Fig. 7 The wire direction (rotated 90° from the position shown in fig. 6)

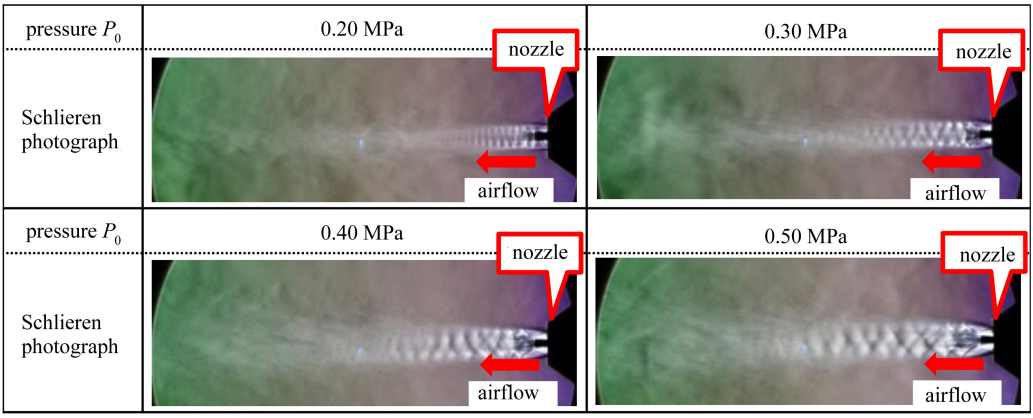

Fig. 8 The Schlieren photographs

2 CFD approach

2.1 Computation method

With the general purpose thermo-fluid simulation software SC/Tetra, we applied a numerical simulation model to the plume analysis. For advective term data calculation, Rotated-RHLL method[7] which is the default solver specified for the software was used. The Rotated-RHLL solver, a method that combines the HLL and Roe solvers, is capable of capturing shock waves, expansion waves, and contact surfaces with high resolution while not causing carbuncle phenomena in which impact wave surfaces tend to be unstable. For diffusion term calculation and time integration, the alpha-damping scheme[8-10] and the defect correction method were used respectively, and the SST k-ω was used for the turbulence model. The SST k-ω turbulence model is known to behave well in analyses of flows that involve separation and obtain higher accuracy for separated flows than typical turbulence models including k-ω.

2.2 Computation model and conditions

Fig. 9 shows the computational model, which calculated the region nearer to the jet outlet than to the tank where the Schlieren images of jet plumes were taken during the experiment. The simulation let the total pressure at the measured temperature represent a variable inflow parameter. For the model, a cylindrical open space was provided around a 6 mm diameter nozzle. All the walls of the cylindrical open space were considered as the outlets of the airflow, and we let the total pressure on the wall surfaces (i.e., atmospheric pressure) at the measured temperature represent a variable outflow parameter. These parameters are given in table 2.

Table 2 Boundary conditions

inflow condition	outflow condition	wall surface
total pressure regulation(0.4 MPa at 39 ℃)	surface pressure regulation(0.0 MPa at 29 ℃)	stationary wall

2.3 Computer used for analysis

The system has 32 computation nodes, and the storage size per node and CPU config-

uration per node are given in table 3. The FDR (fourteen data rate, 14 Gb/s data rate per lane) InfiniBand was used for data interconnection of CX2550M1 computation nodes, and the 2 CPUs within each CX2550M1 were interconnected via 9.6 GT/s (gigatransfer per second) QuickPath Interconnect (QPI).

Table 3 Configuration of the computing system

OS	CPU	memory	number of nodes	sharing storage	interconnection
RedHatEL6.5 (management node and file server) CentOS6.5 (computation node)	Intel Xeon E5-2680v3 (2.5 GHz) ×2, 24 cores/node	64 GB/node	32	FEFS 44 TB	InfiniBand FDR (56 Gbps)

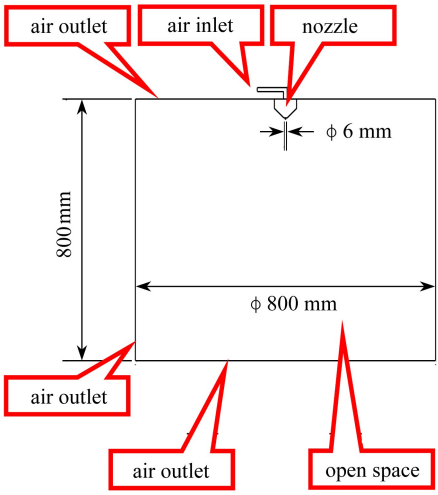

Fig. 9 The analysis model

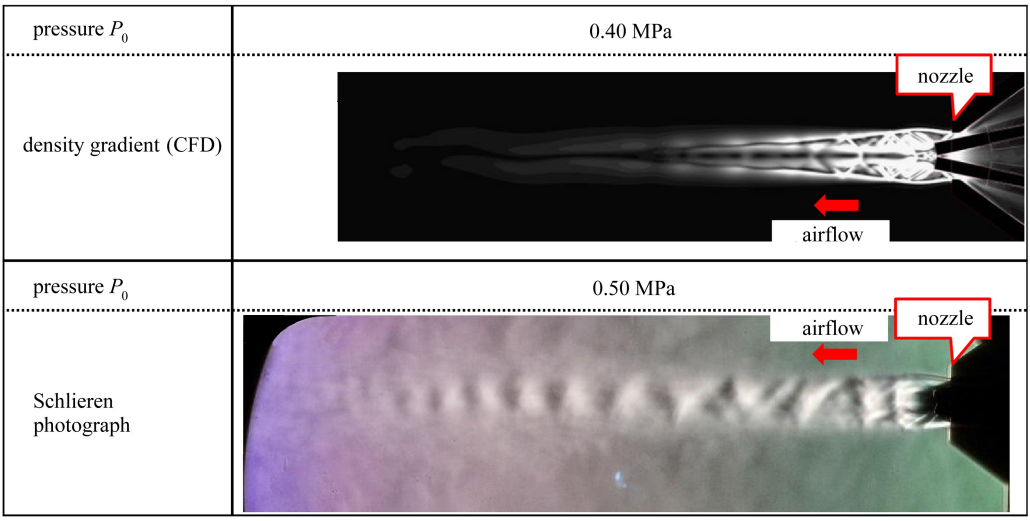

Fig. 10 Density gradients and Schlieren photographs (the wires were positioned in the direction shown in fig. 6)

3 Results of computation

Fig. 10 shows the analysis results (i.e., density gradients) at the inflow parameter of 0.4 MPa. Pressure drops at the coupler and air hoses during the experiment were taken into account at the inflow parameter of 0.4 MPa. The wires were positioned so they were fed in the direction shown in fig. 6. The results of this CFD indicate that the airflow compression (white portions in the figure) takes place at the nozzle aperture. After that, the airflow goes through a cycle of repeated expansion and compression in a damping pattern. Lastly, fig. 11 shows the results of the CFD with the wires positioned in the direction shown in fig. 7. As indicated in the Schlieren photography, compressions in the upper and lower regions of the wires close to the nozzle aperture are observed, then, the airflow repeats the cycle of expansion and compression in a damping pattern.

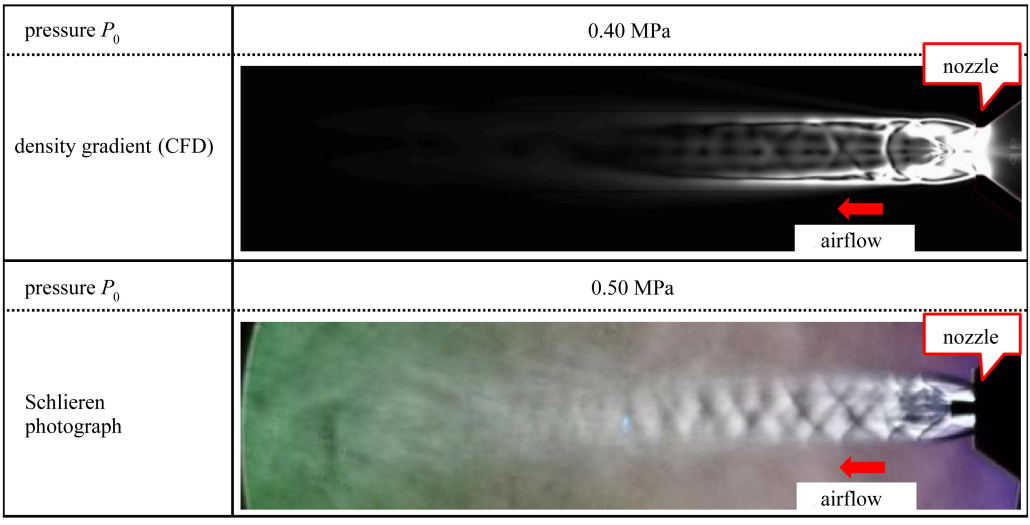

Fig. 11 Density gradients and Schlieren photographs (the wires were positioned in the direction shown in fig. 7)

4 Conclusions

In this study, we aimed to elucidate the properties of the jet plume spurting from the arc spray gun nozzle, and the data presented here supports the following points:

1) The main results of our Schlieren photography are that the direction of wires has effect on jet plume properties and that shock waves are formed in the upper and lower regions of the wire adjacent to the nozzle aperture, i.e., the area in which 2 wires are close enough to merge as one.

2) The results of the CFD suggest that airflow is compressed at the nozzle aperture, then, repeats the cycle of expansion and compression in a damping pattern.

3) The formation of flow compression/expansion as well as plume width varies depending on the direction of wires.

References:

[1] Watanabe T, Usui M. Effect of atomizing gas on oxidation of droplets in wire arc spraying[J]. *Journal of the Japan Institute of Metals*, 1999, **63**(1): 98-102.

[2] Kawase R, Kureishi M, Minehisa S. Relation between arc spraying condition and adhesion strength of sprayed coatings[J]. *Journal of the Japan Welding Society*, 1983, **1**(2/3): 119-124.

[3] Kawase R, Kureishi M, Maehara K. Arc phenomenon and wire fusion in arc spraying[J]. *Journal of the Japan Welding Society*, 1984, **15**(2): 34-39.

[4] Kawase R, Kureishi M. Fused metal temperature in arc spraying[J]. *Journal of the Japan Welding Society*, 1984, **2**(3): 52-58.

[5] Kawase R, Kureishi M. Relation between adhesion strength of sprayed coating and fused metal temperature[J]. *Journal of the Japan Welding Society*, 1985, **16**(2): 165-169.

[6] Kato Koken Co Ltd[Z/OL]. [2016-12-01]. http://www.kokenmpc.co.jp/english/index.html.

[7] Nishikawa H, Kitamura K. Very simple, carbuncle-free, boundary-layer-resolving, rotated-hybrid Riemann solvers[J]. *Journal of Computational Physics*, 2008, **227**(4): 2560-2581.

[8] Nishikawa H. Beyond interface gradient: a general principle for constructing diffusion schemes [C]//*40th Fluid Dynamics Conference and Exhibit*. Chicago, Illinois, 2010: AIAA 2010-5093.

[9] Nishikawa H. Robust and accurate viscous discretization via upwind scheme—I: basic principle[J]. *Computers & Fluids*, 2011, **49**(1): 62-86.

[10] Nishikawa H. Two ways to extend diffusion schemes to Navier-Stokes schemes: gradient formula or upwind flux[C]//*20th AIAA Computational Fluid Dynamics Conference*. Honolulu, Hawaii, 2011: AIAA 2011-3044.

电弧喷涂的喷嘴射流研究

玉城怜士[1], 山川胜史[2]

(1. 日本 Daihen 集团, 兵库县 神户市 东滩区 6580033, 日本;
2. 京都工艺纤维大学, 京都 松岬 左京区 6068585, 日本)

摘要: 紧邻电弧喷涂枪喷嘴产生的喷射尾流对生成涂层的性质有着显著的影响.采用计算流体力学(CFD)和纹影摄影技术阐明了喷射尾流的性质.纹影图像的检查结果显示,尾流的性质和宽度取决于用于热喷涂的丝材的方向.通过 CFD 方法,观察到激波在喷嘴孔口之后迅即形成,然后在下游尾流中衰减.

关 键 词: 电弧喷涂; 激波; 压缩; 膨胀

引用本文/Cite this paper:

TAMAKI Ryoji, YAMAKAWA Masashi. Study on the nozzle jet in arc spraying[J]. *Applied Mathematics and Mechanics*, 2016, **37**(12): 1394-1402.

玉城怜士, 山川胜史. 电弧喷涂的喷嘴射流研究[J]. 应用数学和力学, 2016, **37**(12): 1394-1402.